Baseline Studies of the Clay Minerals Society Source Clays: Infrared Methods

Article *in* Clays and Clay Minerals · January 2001

DOI: 10.1346/CCMN.2001.0490508

1 author:

Jana Madejova
Slovak Academy of Sciences
131 PUBLICATIONS **6,366** CITATIONS

SEE PROFILE

Clays and Clay Minerals, Vol. 49, No. 5, 410–432, 2001.

BASELINE STUDIES OF THE CLAY MINERALS SOCIETY SOURCE CLAYS: INFRARED METHODS

JANA MADEJOVÁ AND PETER KOMADEL

Institute of Inorganic Chemistry, Slovak Academy of Sciences, SK-842 36 Bratislava, Slovakia

INTRODUCTION

Infrared (IR) spectroscopy has a long and successful history as an analytical technique and is used extensively (McKelvy *et al.*, 1996; Stuart, 1996). It is mainly a complementary method to X-ray diffraction (XRD) and other methods used to investigate clays and clay minerals. It is an economical, rapid and common technique because a spectrum can be obtained in a few minutes and the instruments are sufficiently inexpensive as to be available in many laboratories. An IR spectrum can serve as a fingerprint for mineral identification, but it can also give unique information about the mineral structure, including the family of minerals to which the specimen belongs and the degree of regularity within the structure, the nature of isomorphic substituents, the distinction of molecular water from constitutional hydroxyl, and the presence of both crystalline and non-crystalline impurities (Farmer, 1979).

The interpretation of the absorption spectra of the Source Clays in the middle-IR (MIR) region (4000–400 cm^{-1}) given here follows those of Farmer and Russell (1964), Farmer (1974a, 1979) and Russell and Fraser (1994). In addition, reflectance spectra in the near-IR (NIR) region (11,000–4000 cm^{-1}), where overtones and combination vibrations occur, are included. These spectra provide information on structural OH groups and H_2O in clay minerals (Bishop *et al.*, 1994; Frost and Johansson, 1998; Petit *et al.*, 1999a) which may not be clearly observed in the MIR spectra. Small changes in stretching and bending band positions are additive in the combination bands, thereby making them more readily differentiated (Post and Noble, 1993).

Dispersive IR spectrometers are slowly being replaced by quicker and more sensitive Fourier transform (FT) instruments (Rintoul *et al.*, 1998). The greater sensitivity of the FTIR spectrometers is related to the continuous detection of the entire transmitted energy simultaneously, using interferometers, and rapid Fourier transformation of the interferogram into a spectrum (Koenig, 1992; Russell and Fraser, 1994). The increased sensitivity of FTIR spectrometers led to the development and recent broad application of reflectance techniques, such as ATR and DRIFT (Griffiths and de Haseth, 1986).

Attenuated total reflectance (ATR) has been used as a sampling technique for IR spectroscopy since it was developed for dispersive instruments. However, only the increased sensitivity of FTIR spectrometers makes the ATR method a simple and routine technique (Rintoul *et al.*, 1998). ATR has been used extensively to investigate adsorption of organic substances on minerals. The main advantage in clay-minerals research is that ATR allows the measurement of the spectra of dispersions, gels or pastes (Hunter and Bertsch, 1994; Shewring *et al.*, 1995; Yan *et al.*, 1996a,b).

Diffuse reflectance infrared Fourier transform (DRIFT) is widely used in the analysis of solids and powders and generally requires little sample preparation. The DRIFT method is a rapid technique for analyzing samples without interference related to sample preparation. Its use is limited somewhat by interference effects created by particle size and incident IR wavelengths, which may appear toward the low-frequency region, normally below 1200 cm^{-1} for clays. To minimize such effects, the clay is mixed with KBr to obtain good DRIFT spectra in the 1200–400 cm^{-1} region. The DRIFT technique is most appropriate in the NIR region, where no dilution of the sample is necessary. Thus, DRIFT is suitable for studies of hydroxyl vibrations of clays in both MIR and NIR regions (Frost and Johansson, 1998).

This paper summarizes data from FTIR spectra in the NIR and MIR regions (11,000–400 cm^{-1}) of many of the Source Clay samples, using both transmission and reflectance techniques.

METHODS

The FTIR spectra were obtained using a Nicolet Magna 750 FTIR spectrometer, equipped with an IR source, KBr beam splitter, and DTGS KBr detector for MIR measurements, and a white light source, CaF_2 beam splitter and PbSe detector for NIR measurements. For each sample, 128 scans in the 11,000–4000 cm^{-1} (NIR) and 4000–400 cm^{-1} (MIR) spectral ranges were recorded with a resolution of 4 cm^{-1}. Fine fractions of the samples were prepared and described by Costanzo (2001), and these samples were analyzed as received.

The KBr pressed-disc technique is most widely used for preparing a solid sample for routine scanning of the spectra in the MIR region. Samples of 2 and 0.5 mg were dispersed in 200 mg of KBr to record optimal

spectra in the regions of 4000–3000 and 4000–400 cm^{-1}, respectively. The diameter of the pellets, pressed from samples, was 13 mm. Discs for the 4000–3000 cm^{-1} region were heated in a furnace overnight at 150°C to minimize the water adsorbed on KBr and the clay sample.

In addition to KBr discs, self-supporting films were prepared for selected samples. This technique avoids any interaction between the clay sample and KBr, which may even occur at room temperature (Russell, 1974). A 2% suspension of the sample in water was pipetted onto a thin polyethylene sheet and allowed to evaporate to dryness overnight at room temperature. The film was peeled from the polyethylene by drawing it over a sharp edge. A 13 mm diameter circle cut from the film was placed normal to the IR beam in the sample holder of a transmission cell, which permitted heating to 200°C.

The ATR spectra in the MIR region were obtained using MIRacle, the single reflection horizontal ATR accessory from PIKE Technologies (Madison, WI, USA). The sampling plate of the device features a small round ZnSe crystal, which allows reliable analysis of small samples in the spectral range of 20,000 to 650 cm^{-1}. The powder sample was placed on the ZnSe crystal and pressed with a micrometer-controlled compression clamp. Good contact between the sample and crystal is needed to obtain high-quality spectra.

The DRIFT spectra in the NIR region were obtained using a diffuse-reflectance accessory 'Collector' from Spectra-Tech (Shelton, CT, USA). Samples were analyzed at room temperature without dilution in KBr. Samples were poured loosely into a sample cup of ~1 mm depth and 3 mm diameter. The powder was assumed to have random orientation. Freshly prepared MgO was used for background measurement.

Comparison of the sample-preparation methods

To provide adequate characterization of the samples, both transmission and reflectance techniques were utilized. The advantages and disadvantages of methods commonly used to obtain spectra in the MIR region are discussed briefly for SWy-2 and Syn-1 samples. Figure 1 shows the transmission spectra of SWy-2 where two concentrations of the sample were used to prepare the KBr pellet (Figure 1a). The pellet with the 0.5 mg sample was measured immediately after pressing, whereas the disc with the 2 mg sample was heated overnight at 150°C to minimize adsorbed water, thereby providing higher resolution in the OH-stretching region (3800–3200 cm^{-1}). More intense bands were observed for the greater concentration of SWy-2. However, for some samples this greater concentration may result in total absorption of radiation in the region 1200–1000 cm^{-1}. Complete spectra obtained with the 0.5 mg sample in KBr, and spectra of the OH-stretching region with the 2 mg sample as inserts, are presented for all Source Clay samples in this paper.

The pressing of KBr with a clay to prepare the KBr pellet may alter the spectrum through exchange of K into the structure (*e.g.* K–NH_4 exchange, see below). The self-supporting film technique allows study of samples without a KBr matrix (Figure 1b). Slight heating (15 min at 150°C) of the film of SWy-2 completely eliminated the band near 3400 cm^{-1} related to H_2O adsorbed on the sample, and a well-resolved band at 3629 cm^{-1} assigned to OH-stretching vibrations of structural hydroxyls remained. This technique was also useful for the 950–800 cm^{-1} region, where well-resolved absorption bands are present. In contrast, spectral features near 1000 cm^{-1} were not obtained because of the total absorption of radiation; it is difficult to obtain sufficiently thin self-supporting films. Further details on transmission IR techniques were discussed by Russell (1974) and Russell and Fraser (1994).

Reflectance spectra of SWy-2, obtained by DRIFT and ATR techniques, are shown in Figure 2. The DRIFT spectra were transformed using the Kubelka-Munk algorithm, which allows the intensity of the measured IR spectrum to be linearly related to the sample concentration. The DRIFT spectrum of the pure SWy-2 sample in the region below 1200 cm^{-1} exhibits the major limitation of this technique, where spectral features unusual for transmission spectra appear. The origin of this effect is understood if the diffuse-reflectance phenomenon is considered. Where IR radiation is directed onto the surface of a solid sample, two types of reflected energy occur, *i.e.* specular reflectance and diffuse reflectance. The specular component is radiation, which reflects directly from the sample surface and has no absorptive interaction with the sample. Diffuse reflectance results from penetration into the sample and interaction with the particles. Thus, this latter radiation contains spectral information on IR absorption. Diffuse reflection and specular reflection are mixed and cannot be separated spatially, although a diffuse-reflectance accessory optimizes diffuse-reflected energy and minimizes the specular component. Specular reflectance can produce derivative-shaped peaks or apparent absorbance dips, or so-called 'restrahlen bands' (Griffiths, 1983). Clay minerals show 'restrahlen bands' in the region below 1200 cm^{-1}, where Si–O vibrations absorb most of the radiation and the greatest contribution to signal intensity comes from the specular component. However, with modern component analysis techniques, spectra containing a specular component can be analyzed and various minerals in mixtures are differentiated easily (Janik *et al.*, 1998). Such effects can also be minimized by applying Kramers-Kronig relations (Griffths and de Haseth, 1986) or simply by mixing the sample with KBr at about the 10% level. The DRIFT spectrum of a diluted sample is similar to that of a KBr-pellet sample (com-

pare Figure 1, KBr and Figure 2, DRIFT). However, the advantage of minimal sample preparation is lost. On the other hand, DRIFT preferentially probes many highly reflecting minerals (non-smectite), *e.g.* carbonates, oxides and others, and thus is a useful tool for identifying impurities.

The ATR spectroscopy utilizes the phenomenon of total internal reflection. The internal reflectance element, which is a prism of IR-transmitting material of high refractive index (*e.g.* ZnSe), is the main component of an ATR cell. The IR radiation entering a crystal undergoes total internal reflection where the angle of incidence at the interface between the sample and the crystal is greater than the critical angle. When a sample is brought into contact with the surface of the ATR crystal, the evanescent wave will be attenuated in the regions of the IR spectrum where the sample absorbs energy.

Well-resolved and sharp bands are present in the ATR spectrum of the pure SWy-2 sample (Figure 2, ATR). The positions of the bands in the regions of 4000–3000 and 950–600 cm^{-1} are very similar to those found in the KBr-pellet spectrum. The observed frequencies of the Si–O stretching vibrations near 1000 cm^{-1} are shifted slightly downward from those observed in IR transmission spectroscopy as a result of the optical physics of the system (Koenig, 1992; Rintoul *et al.*, 1998). The ATR is a rapid, non-destructive technique and is a very useful first step to characterize minerals. This technique greatly simplifies sample preparation and, in many cases, makes the pressing of KBr pellets unnecessary. Therefore, ATR spectra for all Source Clay samples are shown here.

The importance of the selection of the appropriate technique for a particular problem is illustrated in Figure 3, where transmission and reflectance spectra for the Syn-1 sample are compared. Syn-1 is a synthetic mica-montmorillonite, containing NH_4^+ in the interlayer. Although the ATR, DRIFT and Film spectra are similar, the KBr and KBr-heated spectra differ in the regions of 3400–2800 cm^{-1} and near 1400 cm^{-1}, where the bands related to stretching and deformation vibrations of NH_4^+ occur (Chourabi and Fripiat, 1981; Petit *et al.*, 1999b). The KBr-pellet spectra indicate that an exchange of NH_4^+ by K^+ from KBr occurs even at room temperature.

RESULTS AND DISCUSSION

Two sets of spectra in the MIR region, using the pressed KBr pellet and ATR sampling techniques, and DRIFT spectra in the NIR region are presented for each Source Clay studied. The peak positions observed in the MIR spectra and their assignments (Farmer 1974a, Russell and Fraser, 1994) are listed in Tables 1–7. The band assignment in the NIR region is discussed in more detail because this spectral region is less frequently reported in the literature than the MIR region.

KGa-1b, and KGa-2 kaolinites, Georgia

MIR region. Figures 4 to 7 show IR spectra of the KGa-1b and KGa-2 kaolinites; the assignment of the bands given in Table 1. The spectra of both samples show strong resemblance over the entire MIR region, indicating that this technique is not sufficiently sensitive to illustrate clearly the different kinds of defects in these two kaolinites.

NIR region. The bands present in the NIR region are the result of overtones and combinations of fundamental stretching and deformation vibrations. Their theoretical positions can be calculated from the wavenumbers of the bands observed in the MIR region. Major NIR spectral features of KGa-1b and KGa-2 kaolinites are located near 7000 and 4600 cm^{-1}, where the bands corresponding to the first overtone ($2\nu_{OH}$) and combination ($\nu_{OH} + \delta_{OH}$) vibration modes of OH groups are observed (Figures 8 and 9). Analogous to MIR spectra, the NIR spectra of both kaolinites are very similar, therefore only the assignment of the bands in KGa-1b spectrum is discussed. Two strong bands at 7173 and 7065 cm^{-1} are assigned to the $2\nu_{OH}$ overtones of the OH-stretching fundamental modes of inner-surface (ν_{OH} = 3694cm^{-1}) and inner (ν_{OH} = 3620 cm^{-1}) hydroxyl groups, respectively (Petit *et al.*, 1999a). A less resolved doublet at 7141 and 7113 cm^{-1} is related to overtones of inner-surface OH groups observed at 3669 and 3653 cm^{-1} in the MIR region. The strong band at 4527 cm^{-1} and the less intense one at 4624 cm^{-1} correspond to the combination of OH-stretching (3620 and 3694 cm^{-1}) and deformation (915 and 938 cm^{-1}) vibrations of AlAlOH groups. Spectral features similar to those near 7000 and 4600 cm^{-1}, *i.e.* a sharp band with a smaller component on its high-frequency side, are also observed near the 9000 and 5500 cm^{-1} regions, thus indicating that OH vibrations are probably involved in these vibration modes. It appears that the band at 9256 cm^{-1} arises from the $2(\nu_{OH} + \delta_{OH})$ vibration mode of OH groups observed at 3694 and 938 cm^{-1} in the MIR, whereas the band at 9054 cm^{-1} is related to $2(\nu_{OH} + \delta_{OH})$ of the 3620 and 915 cm^{-1} bands. The combination mode ($\nu_{OH} + 2\delta_{OH}$) gives the bands at 5494 cm^{-1} (ν_{OH} = 3694 cm^{-1}, δ_{OH} = 938 cm^{-1}) and at 5421 cm^{-1} (ν_{OH} = 3620 cm^{-1}, δ_{OH} = 915 cm^{-1}). The 10,335 cm^{-1} band may be attributed to the second overtone ($3\nu_{OH}$) of OH-stretching fundamental modes of Al_2OH groups (ν_{OH} = 3620 cm^{-1}). The band at 5238 cm^{-1} is caused by a combination of stretching and bending modes ($\nu_w + \delta_w$) of adsorbed H_2O. The bands observed between 4300 and 4000 cm^{-1} are probably combinations of OH-stretching bands of kaolinite with lattice deformation vibrations (Hunt and Salisbury, 1970; Hunt *et al.*, 1973).

In addition to the bands observed in the NIR spectra of KGa-1b, the KGa-2 spectrum shows an inflexion near 7015 cm^{-1} and a small band at 4465 cm^{-1} (Figure 9). These bands, assigned in accordance with suggestions by Delineau *et al.* (1994) to the first overtone and combination modes of stretching and bending vibrations of AlFeOH groups (at 3598 and 875 cm^{-1}, respectively; unresolved in the MIR spectra, Figures 6 and 7), indicate the presence of some structural Fe in KGa-2.

SWy-2, montmorillonite, Wyoming

MIR region. Figures 10 and 11 show the KBr-pellet and ATR spectra of the Wyoming montmorillonite SWy-2. The positions and assignments of the bands are listed in Table 2. In addition to the bands common to all dioctahedral montmorillonites, diagnostic bands of quartz, present as an impurity in this sample, are observed at 798 and 778 cm^{-1}. Quartz admixture was also found by XRD analysis (Chipera and Bish, 2001).

NIR region. The NIR spectrum of SWy-2 shows a complex band near 7080 cm^{-1} assigned to the overtone ($2\nu_{OH}$) of the structural OH-stretching mode and the overtone of H_2O ($2\nu_{w'}$) bound to surface oxygens of the tetrahedral sheets (Figure 12). The shoulder at 6852 cm^{-1} is assigned to H_2O molecules involved in strong hydrogen bonds ($2\nu_w$). The small sharp band at 7168 cm^{-1} assigned to $2\nu_{OH}$ (for ν_{OH} = 3695 cm^{-1}) indicates traces of kaolinite in this sample. The NIR spectral region can be more useful for detection of kaolinite impurity than the MIR region where the minor inflexion near 3695 cm^{-1} can hardly be distinguished from the main OH band at 3632 cm^{-1} (Figure 10). Small bands at 9077 and 8680 cm^{-1} correspond to $2(\nu_{OH} + \delta_{AlAlOH})$ and $(2\nu_{w'} + \delta_w)$ combinations. The broad band near 10,530 cm^{-1} is believed to be related to second overtones of variously bound H_2O molecules in the sample. The spectral pattern of the clay in this as well as in the 8000–7200 cm^{-1} region is overlapped by adsorption of water vapor present in air. In the region below 6000 cm^{-1}, the spectrum of SWy-2 montmorillonite exhibits a strong band owing to the combination of the stretching and bending vibrations of water at 5255 cm^{-1} and a band at 4534 cm^{-1} characteristic of the ($\nu_{OH} + \delta_{AlAlOH}$) combination mode (Figure 12). A slight shoulder near 4470 cm^{-1} corresponds to the ($\nu_{OH} + \delta_{AlFeOH}$) combination mode. The spectral features near 4100 cm^{-1} were assigned to be combinations of structural OH-stretching vibrations with Si–O deformation vibrations (Hunt and Salisbury, 1970).

SAz-1, montmorillonite, Arizona

MIR region. The KBr-pellet and ATR spectra of SAz-1 (Figures 13 and 14; Table 3), reflect the lower Fe and higher Mg content of this montmorillonite in comparison with SWy-2. A weak band at 792 cm^{-1} indicates traces of poorly crystalline silica.

NIR region. The NIR spectrum of SAz-1 is like that of SWy-2 (Figures 15, 12). However, in comparison with SWy-2, the positions of the bands of structural OH groups are shifted slightly to lower wavenumbers, in accordance with the positions of OH bands observed in the MIR region.

STx-1, montmorillonite, Texas

MIR region. Figures 16 and 17 show the KBr-pellet and ATR spectra of montmorillonite STx-1. The assignments of the bands are given in Table 4. A weak shoulder at 3692 cm^{-1} indicates traces of kaolinite in the sample. Kaolinite was detected among impurities in the separates obtained during purification of montmorillonite for XRD analysis (Chipera and Bish, 2001). The Si–O stretching band at 1089 cm^{-1} is related to crystalline silica admixtures. The relatively strong band at 794 cm^{-1} together with increased intensity of the 626 cm^{-1} band suggest a cristobalite-like phase impurity. These results are in good agreement with XRD analysis, which confirms opal-CT admixture in this sample (Chipera and Bish, 2001).

NIR region. The NIR spectrum of STx-1 strongly resembles those of SWy-2 and SAz-1 (compare Figure 18 with Figures 12 and 15). A weak band at 7167 cm^{-1} shows the presence of kaolinite in this material.

SHCa-1, hectorite, California

MIR region. The KBr-pellet spectra of hectorite reveal the trioctahedral character of this smectite with an OH-stretching band at 3679 cm^{-1} (Figure 19). The OH-stretching region in the KBr-pellet and ATR spectra shows a pronounced decrease in the 3675 cm^{-1} band intensity in the latter (Figure 20). The particles in the KBr disc are randomly oriented, whereas preferential orientation of particles increases owing to compression of the sample onto the surface of the ATR crystal. Comparison of the OH-band intensities in KBr-pellet and ATR spectra can help to identify the 'octahedral character' of smectites because only the absorptivity of vibrations of OH groups of trioctahedral layer silicates, which are nearly normal to the silicate layers, are sensitive to orientation and show variation in intensity between the two spectra. The absorption bands at 1798, 1430 and 875 cm^{-1} (owing to CO_3 vibrations of calcite) and at 800 cm^{-1} (silica) indicate common admixtures present in hectorite (Figure 19).

NIR region. The NIR spectrum of SHCa-1 hectorite in Figure 21 shows that the trioctahedral character of this smectite can also be distinguished in the NIR region. In the spectra of montmorillonites, the structural OH overtone cannot be resolved from the H_2O band because they both appear near 7060 cm^{-1} (Figures 12,

15, 18). However, in the spectrum of SHCa-1, the structural overtone ($2\nu_{OH}$) occurs at 7191 cm^{-1} and the H_2O band at 7067 cm^{-1}, so they can be distinguished from one another. The diagnostic band of H_2O is seen at 5251 cm^{-1}. The major band at 4329 cm^{-1} corresponds to the combination of OH-stretching (3679 cm^{-1}) and deformation (656 cm^{-1}) vibrations of Mg_3OH groups. The sharp band at 4188 cm^{-1} is tentatively assigned to a ($\nu_{OH} + \nu_{Mg\text{-}O}$) combination mode.

Syn-1, synthetic mica-montmorillonite

MIR region. The KBr-pellet and the ATR spectra of the unheated sample show absorption bands near 3630 and 930 cm^{-1} owing to the vibrations of OH groups coordinated to AlAl pairs (Figures 22 and 23; Table 6). The absorption bands at 820 and 757 cm^{-1}, owing to tetrahedral Al–O out-of-plane and Al–O–Si in-plane vibrations, respectively, are characteristic of muscovite, whereas a band near 620 cm^{-1} is common for montmorillonite.

The absorption bands in the 3300–3000 cm^{-1} and near 1400 cm^{-1} are related to stretching and deformation vibrations of NH_4^+, respectively (Table 6). The IR spectra differ significantly for unheated KBr-pellet, heated KBr-pellet, and ATR spectra. In the unheated sample, a strong band of H_2O at 3438 cm^{-1} dominates the OH-stretching region and only a shoulder near 3119 cm^{-1} indicates the presence of NH_4^+. Overnight heating at 150°C reduced the amount of adsorbed H_2O, and the ammonium band at 3133 cm^{-1} with shoulders at 3287, 3015 and 2831 cm^{-1} was observed in the spectrum (Figure 22). In the NH_4^+ deformation region, two bands at 1434 and 1402 cm^{-1} are present in the KBr-pellet spectrum. The ATR spectrum shows broad bands at 3298, 3047 and 1434 cm^{-1} (Figure 23). Differences between the ammonium band positions in these spectra are related to NH_4^+ migration from the clay into the KBr. The bands near 3130 and 1400 cm^{-1} are related to NH_4Br originating following the exchange of NH_4^+ of the clay by K^+ from KBr. The ATR spectrum (with no diluting matrix) shows the bands at 3298, 3047 and 1434 cm^{-1} related to NH_4^+ present in the interlayers of clay minerals (Chourabi and Fripiat, 1981).

NIR region. Figure 24 shows the NIR spectrum of Syn-1. A reduced intensity of the combination band of H_2O at 5242 cm^{-1} together with disappearance of the H_2O band near 6800 cm^{-1} is characteristic of micaceous minerals and indicates a smaller number of swelling layers in Syn-1 in comparison to montmorillonites. A complex band near 7089 cm^{-1} is related mostly to an overtone ($2\ \nu_{OH}$) of the structural OH-stretching mode with an additional contribution of the ($2\ \nu_{w}$) overtone of H_2O. A sharp band at 7176 cm^{-1} is believed to originate from the $2\ \nu_{OH}$ overtone of the high-frequency OH component, observed in MIR spectra of some muscovite samples near 3660 cm^{-1} (Farmer, 1974b; Besson and Drits, 1997). A combination ($\nu_{OH} + \delta_{OH}$) vibration mode appears at 4584 cm^{-1}. In addition to OH bands, the first overtone ($2\ \nu_{NH_4}$) and combination ($\nu_{NH_4} + \delta_{NH_4}$) vibration modes are observed at 6426 and 4735 cm^{-1}, respectively.

PFl-1, palygorskite, Florida

MIR region. The IR spectra of palygorskite (attapulgite) PFl-1 indicate that this sample has quartz (798 and 776 cm^{-1}) and possibly feldspar (720–500 cm^{-1} region) admixtures (Figures 25 and 26). The structural OH-stretching band at 3615 cm^{-1} together with the well-defined AlAlOH deformation band at 912 cm^{-1} and a slight inflexion near 860 cm^{-1} (AlMgOH) reflect the dominantly dioctahedral character of palygorskite. Pronounced changes occurred in the spectra of the self-supporting film, where the OH-stretching band shifted from 3617 to 3626 cm^{-1} after heating of PFl-1 (Figure 27). A typical feature of palygorskite is the complex nature of absorption bands of H_2O molecules in the 3600–3000 cm^{-1} region, which show considerable modification on drying (Figures 25, 27).

NIR region. The NIR spectrum of PFl-1 shows a sharp band at 7058 cm^{-1} attributed to the overtone ($2\ \nu_{OH}$) of the structural OH-stretching mode (Figure 28). Combination modes ($\nu_{OH} + \delta_{AlAlOH}$) and ($\nu_{OH} + \delta_{AlMgOH}$) give the bands at 4502 and 4436 cm^{-1}, respectively. Several stretching vibration modes of H_2O observed in the MIR region are also reflected in the NIR region, where the bands at 7002 and 6941 cm^{-1} are related to H_2O bound to Al or Mg and a band at 6822 cm^{-1} corresponds to zeolitic water.

ACKNOWLEDGMENTS

The authors acknowledge financial support of the Slovak Grant Agency (Grant 2/4042) and the contribution of US-Slovak Scientific and Technological Program (Grant 94 055) to obtain the FTIR spectrometer. W. P. Gates is acknowledged for his review and helpful comments.

REFERENCES

Besson, G. and Drits, V.A. (1997) Refined relationships between chemical composition of dioctahedral fine-grained mica minerals and their infrared spectra within the OH stretching region. Part I: Identification of the OH stretching bands. *Clays and Clay Minerals*, **45,** 158–169.

Bishop, J.L., Pieters, C.M. and Edwards, J.O. (1994) Infrared spectroscopic analyses on the nature of water in montmorillonite. *Clays and Clay Minerals,* **42,** 702–716.

Chipera, S.J. and Bish, D.L. (2001) Baseline studies of The Clay Minerals Society Source Clays: powder X-ray diffraction analysis. *Clays and Clay Minerals*, **49,** 398–409.

Chourabi, B. and Fripiat, J.J. (1981) Determination of tetrahedral substitutions and interlayer surface heterogeneity from vibrational spectra of ammonium in smectites. *Clays and Clay Minerals,* **29,** 260–268.

Costanzo, P.M. (2001) Baseline studies of The Clay Minerals Society Source Clays: introduction. *Clays and Clay Minerals*, **49,** 372–373.

Delineau, T., Allard, T., Muller, J.P., Barres, O., Yvon, J. and Cases, J.M. (1994) FTIR reflectance *vs.* EPR studies of structural iron in kaolinites. *Clays and Clay Minerals,* **42,** 308–320.

Farmer, V.C. (1974a) *The Infrared Spectra of Minerals.* Monograph **4.** Mineralogical Society, London, 539 pp.

Farmer, V.C. (1974b) The layer silicates. Pp. 331–363 in: *The Infrared Spectra of Minerals* (V.C. Farmer, editor). Monograph, **4.** Mineralogical Society, London.

Farmer, V.C. (1979) Infrared spectroscopy. Pp. 285–337 in: *Data Handbook for Clay Materials and other Non-metallic Minerals* (H. van Olphen and J.J. Fripiat, editors). Pergamon Press, Oxford, UK.

Farmer, V.C. (1998) Differing effects of particle size and shape in the infrared and Raman spectra of kaolinite. *Clay Minerals,* **33,** 601–604.

Farmer, V.C. and Russell, J.D. (1964) The infrared spectra of layer silicates. *Spectrochimica Acta,* **20,** 1149–1173.

Frost, R.L. and Johansson, U. (1998) Combination bands in the infrared spectroscopy of kaolins—a DRIFT spectroscopic study. *Clays and Clay Minerals,* **46,** 466–477.

Griffiths, P.R. (1983) Fourier transform infrared spectrometry. *Science,* **222,** 297–302.

Griffiths, P.R. and de Haseth, J.A. (1986) *Fourier Transform Infrared Spectrometry.* J Wiley & Sons, New York.

Hunt, G.R. and Salisbury, J.W. (1970) Visible and infrared spectra of minerals and rocks: I. Silicate minerals. *Modern Geology,* **1,** 283–300.

Hunt, G.R., Salisbury, J.W. and Lenhoff, C.J. (1973) Visible and infrared spectra of minerals and rocks: VI. Additional silicates. *Modern Geology,* **4,** 85–106.

Hunter, D.B. and Bertsch, P.M. (1994) *In situ* measurements of tetraphenyl degradation kinetics on clay mineral surfaces by IR. *Environmental Science and Technology,* **28,** 686–691.

Janik, L.J., Merry, R.H. and Skjemtad, J.O. (1998) Can mid infrared diffuse reflectance analysis replace soil extractions? *Australian Journal of Experimental Agriculture,* **38,** 681–96.

Koenig, J.L. (1992) Experimental IR spectroscopy of polymers. Pp. 43–76 in: *Spectroscopy of Polymers.* American Chemical Society, Washington, D.C.

McKelvy, M.L., Britt, T.R., Davis, B.L., Gillie, J.K., Lentz, L.A., Leugers, A., Nyquist, R.A. and Putzig, C.L. (1996) Infrared spectroscopy. *Analytical Chemistry,* **68,** 93R–160R.

Petit, S., Madejová, J., Decarreau, A. and Martin, F. (1999a) Characterization of octahedral substitutions in kaolinites using near infrared spectroscopy. *Clays and Clay Minerals,* **47,** 103–108.

Petit, S., Righi, D., Madejová, J. and Decarreau, A. (1999b) Interpretation of the infrared NH_4^+ signal and layer charge characterization of NH_4-clays. *Clay Minerals,* **34,** 543–549.

Post, J.L. and Noble, P.N. (1993) The near-infrared combination band frequencies of dioctahedral smectites, micas, and illites. *Clays and Clay Minerals,* **41,** 639–644.

Rintoul, L., Panayiotou, H., Kokot, S., George, G., Cash, G., Frost, R., Byi, T. and Fredericks, P. (1998) Fourier transform infrared spectroscopy: a versatile technique for real world samples. *Analyst,* **123,** 571–577.

Russell, J.D. (1974) Instrumentation and techniques. Pp. 11–25 in: *The Infrared Spectra of Minerals* (V.C. Farmer, editor). Monograph, **4.** Mineralogical Society, London.

Russell, J.D. and Fraser, A.R. (1994) Infrared methods. Pp. 11–67 in: *Clay Mineralogy: Spectroscopic and Chemical Determinative Methods* (M.J. Wilson, editor). Chapman & Hall, London.

Shewring, N.I.E., Jones, T.G.J., Maitland, G. and Yarwood, J. (1995) Fourier transform infrared spectroscopic techniques to investigate surface hydration processes on bentonite. *Journal of Colloid Interface Science,* **176,** 308–317.

Stuart, B. (1996) *Modern Infrared Spectroscopy,* John Wiley & Sons, New York and Chichester, UK, 180 pp.

Yan, L., Low, P.F. and Roth, C.B. (1996a) Swelling pressure of montmorillonite layers versus H-O-H bending frequency of the interlayer water. *Clays and Clay Minerals,* **44,** 749–756.

Yan, L., Roth, C.B. and Low, P.F. (1996b) Changes in the Si-O vibrations of smectite layers accompanying the sorption of interlayer water. *Langmuir,* **12,** 4421–4429.

E-mail of corresponding author: uachjmad@savba.sk

Table 1. KGa-1b and KGa-2 kaolinites.

KGa-1b			KGa-2	
KBr	ATR	Assignment	KBr	ATR
Position (cm^{-1})			Position (cm^{-1})	
3694	3689	OH stretching of inner-surface hydroxyl groups[1]	3696	3691
3669	3669	OH stretching of inner-surface hydroxyl groups[2]	3668	—
3653	3651	OH stretching of inner-surface hydroxyl groups[2]	3653	3650
3620	3619	OH stretching of inner hydroxyl groups	3621	3619
3457	—	OH stretching of water	3442	—
1635	—	OH deformation of water	1630	—
—	1115	Si–O stretching (longitudinal mode)	—	1114
1102	—	perpendicular Si–O stretching	1105	—
1033	1027	in-plane Si–O stretching	1033	1028
1011	1005	in-plane Si–O stretching	1008	1004
938	937	OH deformation of inner-surface hydroxyl group	937	935
915	912	OH deformation of inner hydroxyl groups	914	912
791	788	Si–O	791	789
755	751	Si–O, perpendicular	754	750
697	681	Si–O, perpendicular	698	684
—	645	Si–O	—	641
541	—	Al–O–Si deformation	540	—
472	—	Si–O–Si deformation	470	—
432	—	Si–O deformation	430	—

[1] In-phase vibration with a transition moment nearly perpendicular to the (001) plane.
[2] Anti-phase vibration with transition moment lying in the (001) plane (Farmer, 1998).

Table 2. SWy-2 montmorillonite.

SWy-2		
KBr	ATR	Assignment
Position (cm^{-1})		
3632[1]	—	OH stretching of structural hydroxyl groups
3627	3626	OH stretching of structural hydroxyl groups
3422[1]	3393	OH stretching of water
1634	1632	OH deformation of water
—	1116	Si–O stretching (longitudinal mode)
1041	1003	Si–O stretching
917	916	AlAlOH deformation
885	885	AlFeOH deformation
842	846	AlMgOH deformation
798	797	Si–O stretching of quartz and silica
778	779	Si–O stretching of quartz
	687	Si–O
620	623	Coupled Al–O and Si–O, out-of-plane
524	—	Al–O–Si deformation
466	—	Si–O–Si deformation

[1] Insert in Figure 10: 2.0 mg sample/200 mg KBr, disk heated overnight at 150°C.

Table 3. SAz-1 montmorillonite.

SAz-1		
KBr	ATR	
Position (cm^{-1})		Assignment
3622[1]	—	OH stretching of structural hydroxyl groups
3620	3610	OH stretching of structural hydroxyl groups
3426[1]	3373	OH stretching of water
1634	1629	OH deformation of water
—	1102	Si–O stretching (longitudinal mode)
1030	992	Si–O stretching
915	913	AlAlOH deformation
842	837	AlMgOH deformation
792	798	Si–O of silica
—	684	Si–O
620	617	Coupled Al–O and Si–O, out-of-plane
520	—	Al–O–Si deformation
465	—	Si–O–Si deformation

[1] Insert in Figure 13: 2.0 mg sample/200 mg KBr, disk heated overnight at 150°C.

Table 4. STx-1 montmorillonite.

STx-1		
KBr	ATR	
Position (cm^{-1})		Assignment
3692[1]		OH stretching of structural hydroxyl groups of kaolinite
3626[1]		OH stretching of structural hydroxyl groups
3622	3618	OH stretching of structural hydroxyl groups
3424[1]	3393	OH stretching of water
1634	1633	OH deformation of water
—	1113	Si–O stretching (longitudinal mode)
1089	—	Si–O stretching of cristobalite
1036	1006	Si–O stretching
915	914	AlAlOH deformation
846	842	AlMgOH deformation
794	791	Si–O stretching of cristobalite
—	687	Si–O
626	623	Coupled Al–O and Si–O, out-of-plane; Si–O of cristobalite
521	—	Al–O–Si deformation
467	—	Si–O–Si deformation

[1] Insert in Figure 16: 2.0 mg sample/200 mg KBr, disk heated overnight at 150°C.

Table 5. SHCa-1 hectorite.

SHCa-1			
KBr	KBr[1] Position (cm^{-1})	ATR	Assignment
3678	3679	3675	OH stretching of structural hydroxyl groups
—	3621	3629	OH stretching of bonded water
3438	3440	3402	OH stretching of water
1798	—	—	combination band of calcite
1630	—	1633	OH deformation of water
1430	—	1421	CO_3 stretching of calcite
1013	—	989	Si–O stretching
875	—	874	out-of-plane bending of calcite
800	—	795	Si–O of silica
710	—	701	Si–O stretching + in-plane bending of calcite
656	—	651	Mg_3OH deformation
524	—	—	Mg–O stretching out of plane
468	—	—	Si–O–Si deformation

[1] Insert in Figure 19: 2.0 mg sample/200 mg KBr, disk heated overnight at 150°C.

Table 6. Syn-1 mica-montmorillonite.

Syn-1			
KBr	KBr[1] Position (cm^{-1})	ATR	Assignment
3633	3641	3629	OH stretching of structural hydroxyl groups
3438	—	—	OH stretching of water
—	3287	3298	NH_4 stretching of NH_4-clay
3119	3133	—	NH_4 stretching of NH_4Br
—	3015	3047	combination band of NH_4
—	2831	—	overtone of NH_4
1635	—	1635	OH deformation of water
1434	—	1434	NH_4 deformation of NH_4-clay
1402	—	—	NH_4 deformation of NH_4Br
1030	—	989	Si–O stretching
929	—	928	AlAlOH deformation
820	—	820	Al–O of muscovite
757	—	753	Al–O–Si of muscovite
702	—	699	Si–O
622	—	616	coupled Al–O and Si–O, out-of-plane
535	—	—	Al–O–Si deformation
475	—	—	Si–O–Si deformation
430	—	—	Si–O

[1] Insert in Figure 22: 2.0 mg sample/200 mg KBr, disk heated overnight at 150°C.

Table 7. PFl-1 palygorskite.

PFl-1			
KBr	KBr[1] Position (cm^{-1})	ATR	Assignment
—	3623	—	OH stretching of structural hydroxyl groups
3615	3610	3613	OH stretching of structural hydroxyl groups
—	3579	3583	OH stretching of water coordinated to Al, Mg
3545	3541	3545	OH stretching of water coordinated to Al, Mg
—	3521		OH stretching of water coordinated to Al, Mg
3417	—		OH stretching of adsorbed and zeolitic water
—	3398	3371	OH stretching of zeolitic water
—	—	3273	Overtone of OH deformation of water
1642	—	1653	OH deformation of water
1194	—	1194	Si–O stretching
1028	—	1019	Si–O stretching
986	—	978	Si–O stretching
912	—	912	AlAlOH deformation
798	—	797	Si–O stretching of quartz
776	—	779	Si–O stretching of quartz
—	—	728	Si–O stretching of feldspar
643	—	643	Si–O stretching of feldspar
512	—	—	Si–O deformation of feldspar
479	—	—	Si–O–Si deformation
428	—	—	Si–O deformation of feldspar

[1] Insert in Figure 25: 2.0 mg sample/200 mg KBr, disk heated overnight at 150°C.

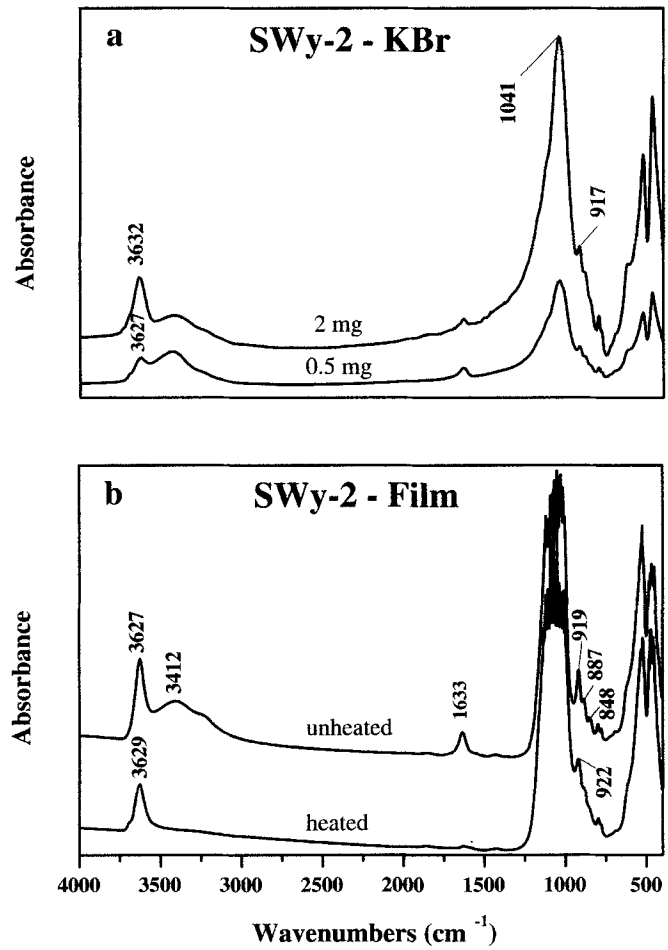

Figure 1. Transmission IR spectra of SWy-2 (montmorillonite) using (a) KBr pellet (0.5 mg sample/200 mg KBr, unheated; 2.0 mg sample/200 mg KBr, heated overnight at 150°C) and (b) self-supporting film-sampling techniques.

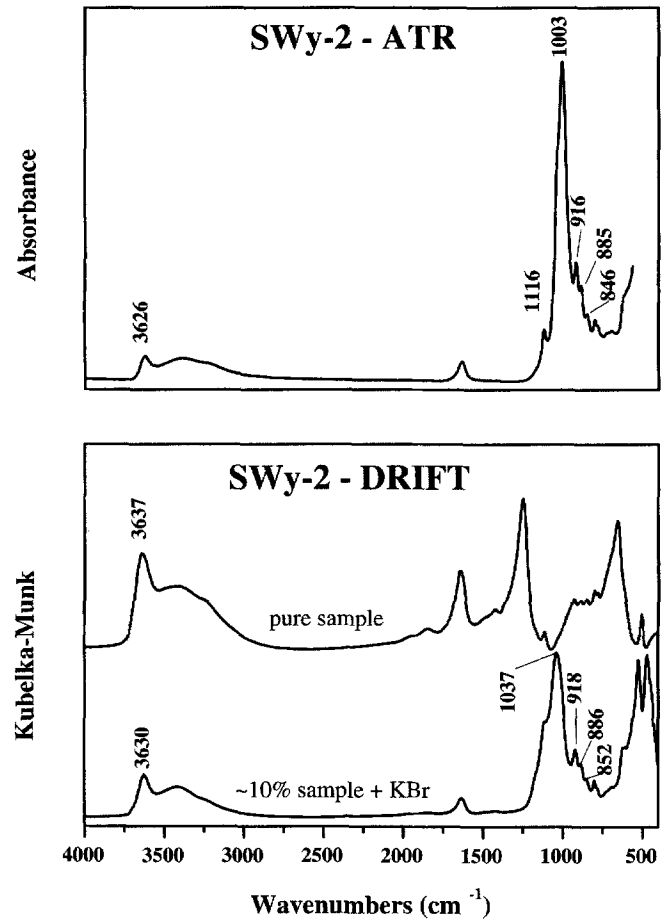

Figure 2. Reflectance IR spectra of SWy-2 (montmorillonite) using ATR and DRIFT techniques.

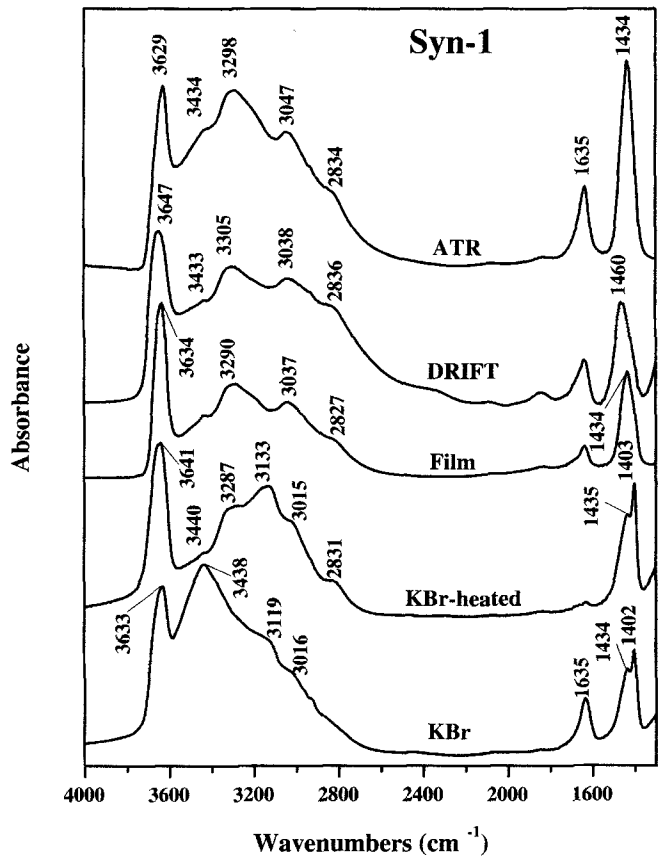

Figure 3. IR spectra of Syn-1 (mica-montmorillonite).

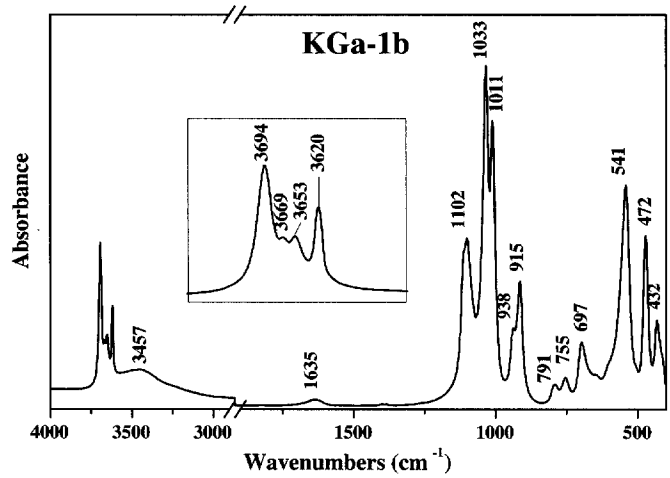

Figure 4. IR spectra of KGa-1b (kaolinite) using 0.5 mg sample/200 mg KBr for 4000–400 cm^{-1}. Insert: 2.0 mg sample/ 200 mg KBr, disk heated overnight at 150°C.

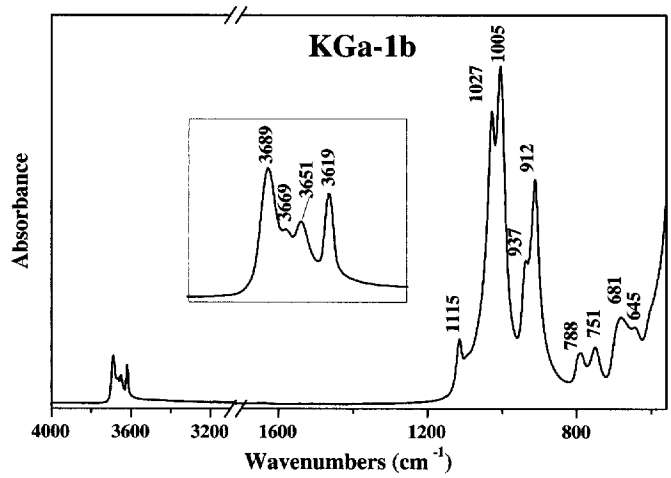

Figure 5. IR spectrum of KGa-1b (kaolinite) using the ATR technique. Insert: the OH-stretching region.

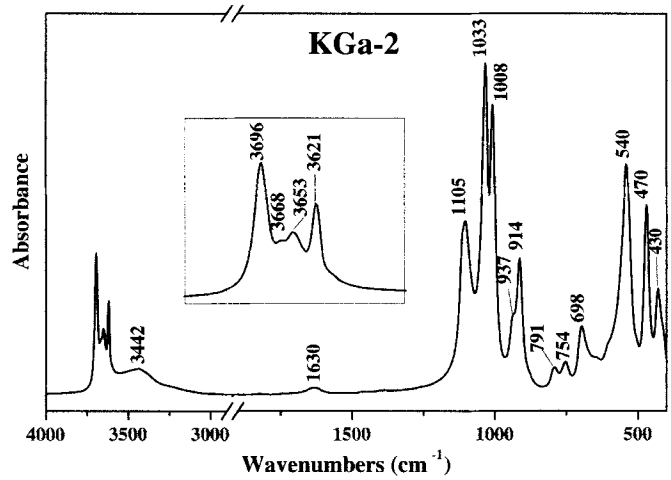

Figure 6. IR spectra of KGa-2 (kaolinite) using 0.5 mg sample/200 mg KBr for 4000–400 cm^{-1}. Insert: 2.0 mg sample/200 mg KBr, disk heated overnight at 150°C.

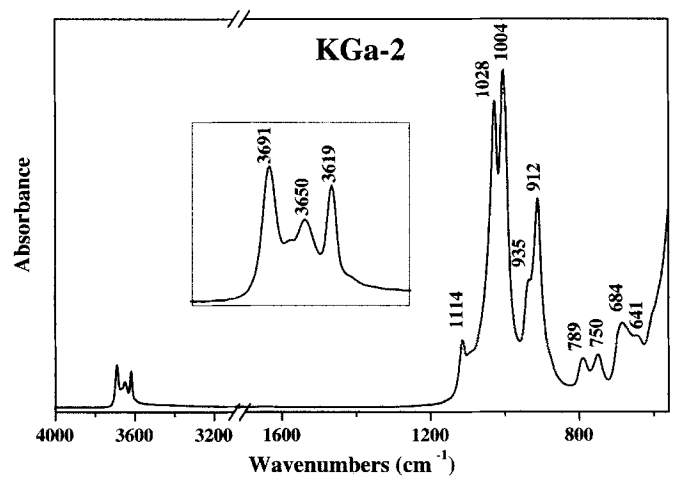

Figure 7. IR spectrum of KGa-2 (kaolinite) using the ATR technique. Insert: the OH-stretching region.

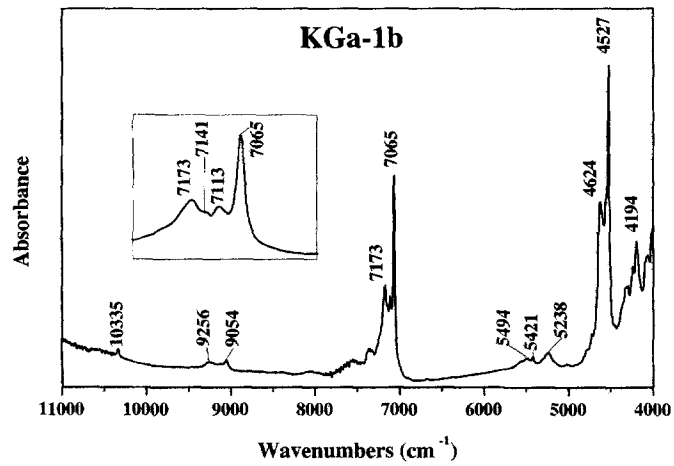

Figure 8. Diffuse-reflectance NIR spectrum of KGa-1b (kaolinite). Insert: the OH overtone region.

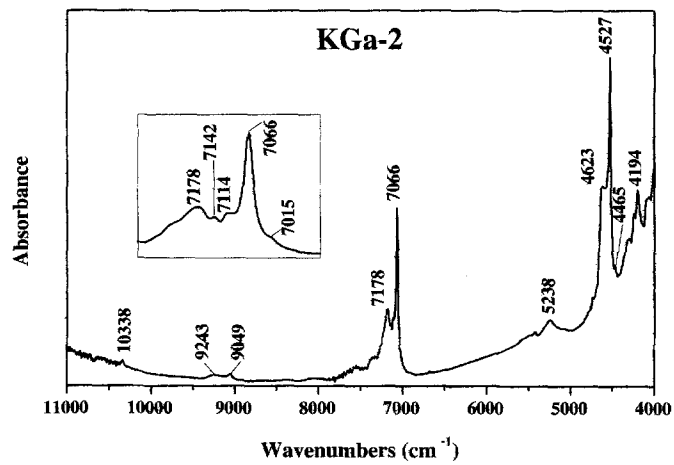

Figure 9. Diffuse-reflectance NIR spectrum of KGa-2 (kaolinite). Insert: the OH overtone region.

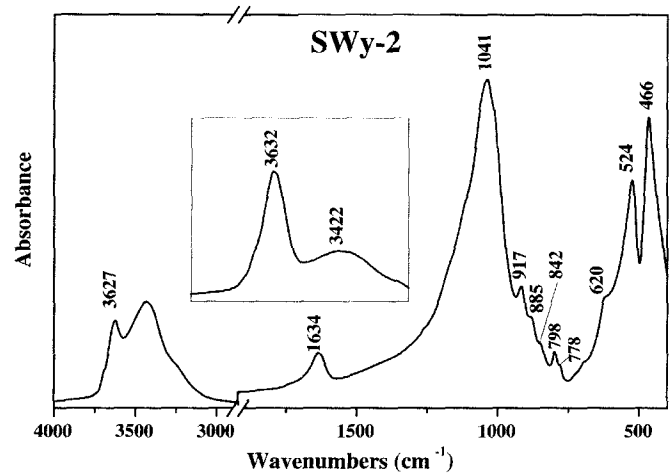

Figure 10. IR spectra of SWy-2 (montmorillonite) using 0.5 mg sample/200 mg KBr for 4000–400 cm^{-1}. Insert: 2.0 mg sample/200 mg KBr, disk heated overnight at 150°C.

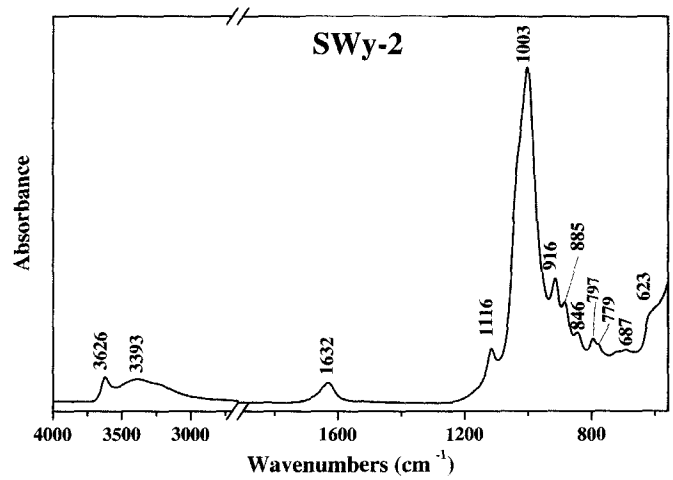

Figure 11. IR spectrum of SWy-2 (montmorillonite) using the ATR technique.

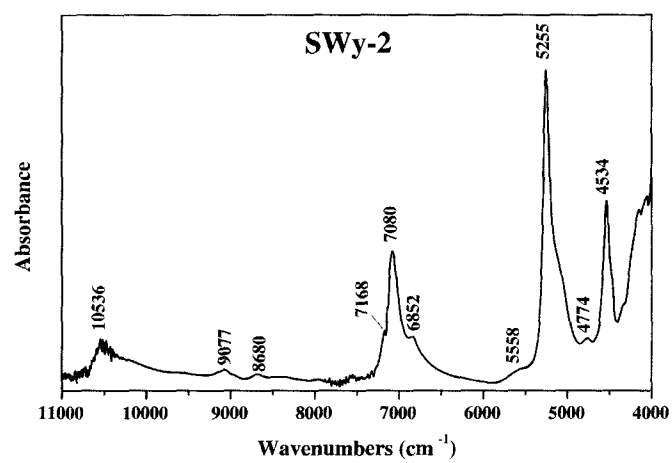

Figure 12. Diffuse-reflectance NIR spectrum of SWy-2 (montmorillonite).

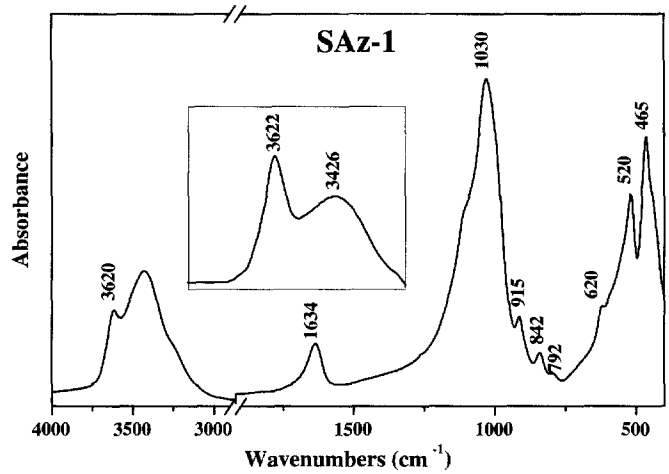

Figure 13. IR spectra of SAz-1 (montmorillonite) using 0.5 mg sample/200 mg KBr for 4000–400 cm^{-1}. Insert: 2.0 mg sample/200 mg KBr, disk heated overnight at 150°C.

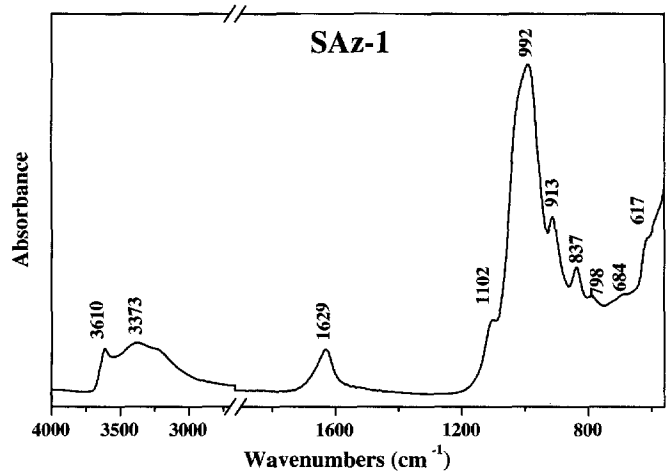

Figure 14. IR spectrum of SAz-1 (montmorillonite) using the ATR technique.

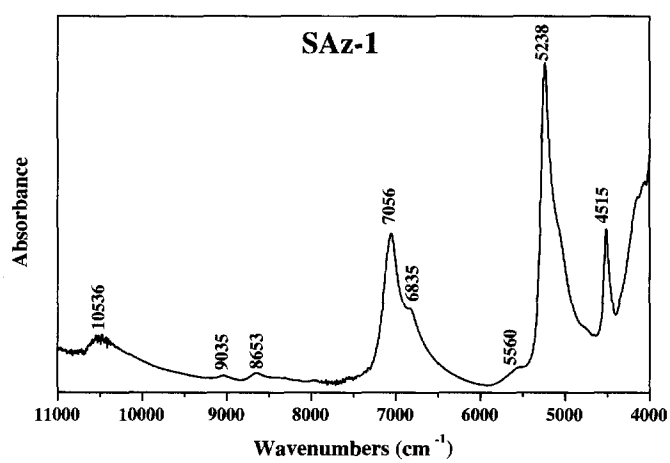

Figure 15. Diffuse-reflectance NIR spectrum of SAz-1 (montmorillonite).

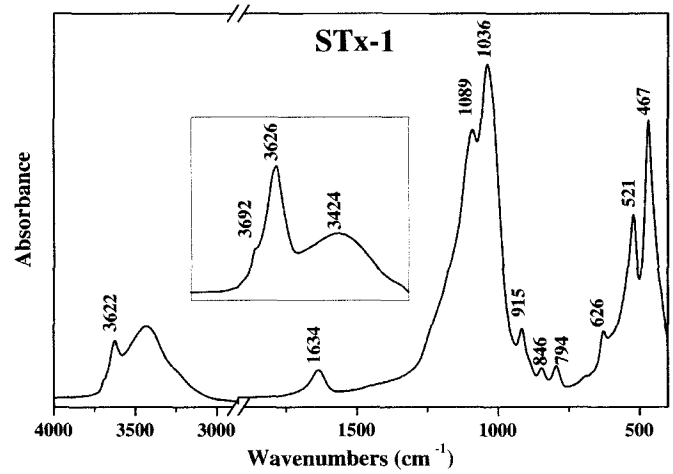

Figure 16. IR spectra of STx-1 (montmorillonite) using 0.5 mg sample/200 mg KBr for 4000–400 cm^{-1}. Insert: 2.0 mg sample/200 mg KBr, disk heated overnight at 150°C.

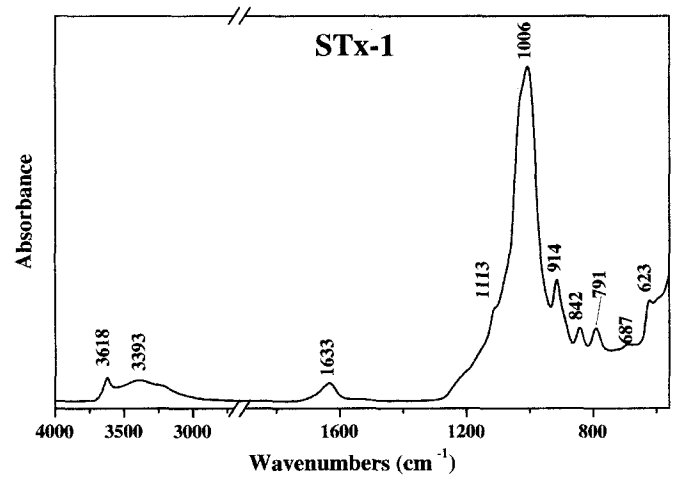

Figure 17. IR spectrum of STx-1 (montmorillonite) using the ATR technique.

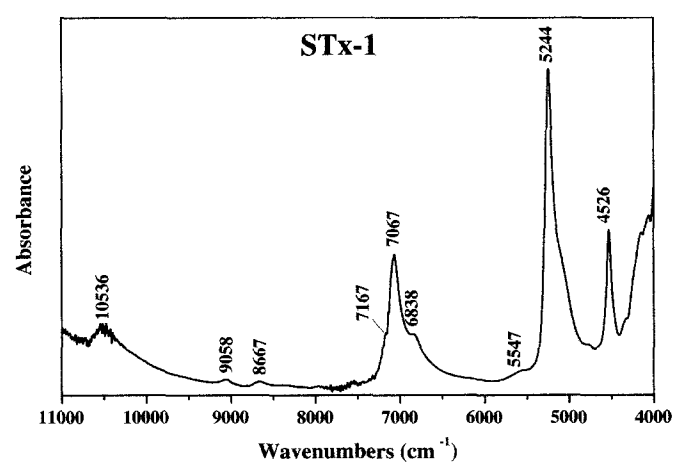

Figure 18. Diffuse-reflectance NIR spectrum of STx-1 (montmorillonite).

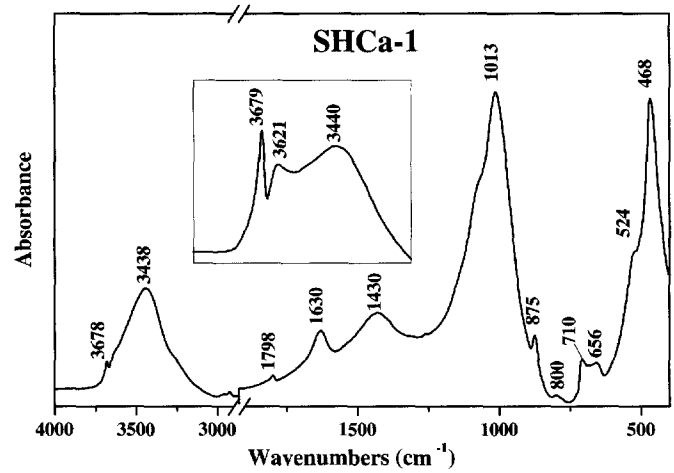

Figure 19. IR spectra of SHCa-1 (hectorite) using 0.5 mg sample/200 mg KBr for 4000–400 cm^{-1}. Insert: 2.0 mg sample/ 200 mg KBr, disk heated overnight at 150°C.

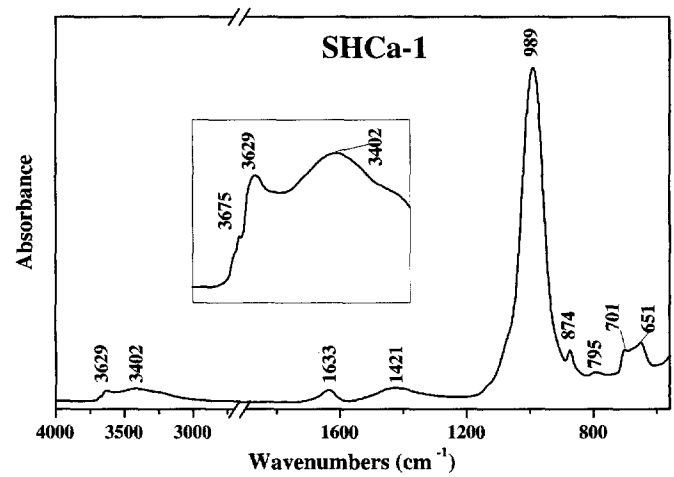

Figure 20. IR spectrum of SHCa-1 (hectorite) using the ATR technique. Insert: the OH-stretching region.

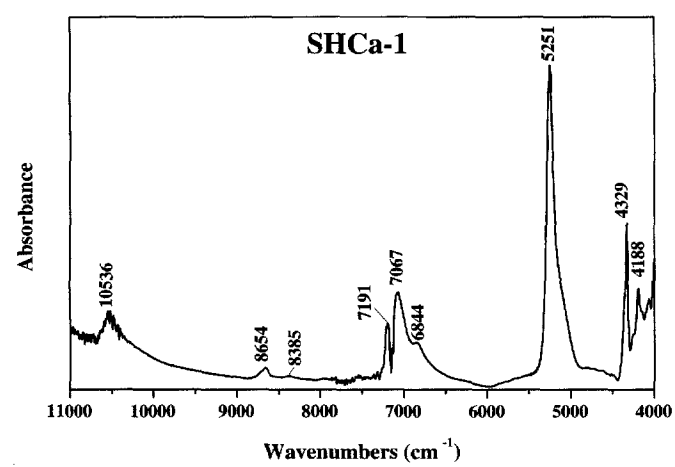

Figure 21. Diffuse-reflectance NIR spectrum of SHCa-1 (hectorite).

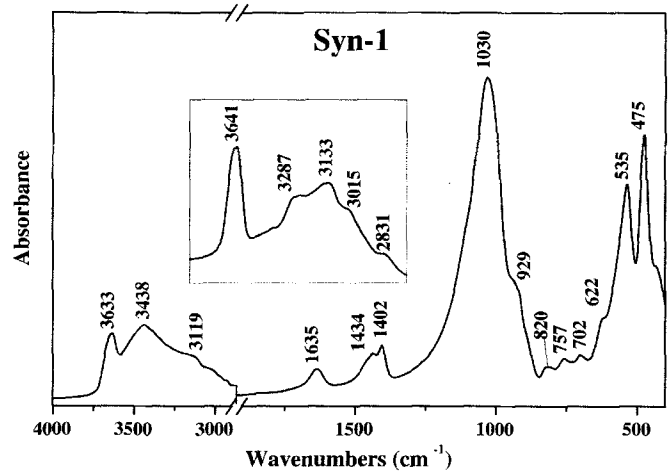

Figure 22. IR spectra of Syn-1 (mica-montmorillonite) using 0.5 mg sample/200 mg KBr for 4000–400 cm^{-1}. Insert: 2.0 mg sample/200 mg KBr, disk heated overnight at 150°C.

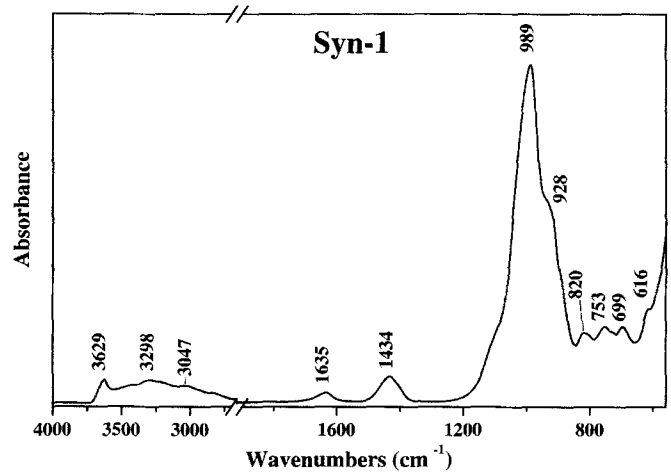

Figure 23. IR spectrum of Syn-1 (mica-montmorillonite) using the ATR technique.

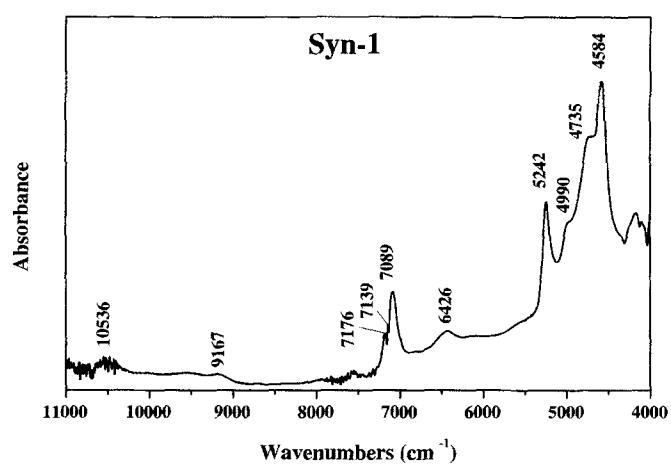

Figure 24. Diffuse-reflectance NIR spectrum of Syn-1 (mica-montmorillonite).

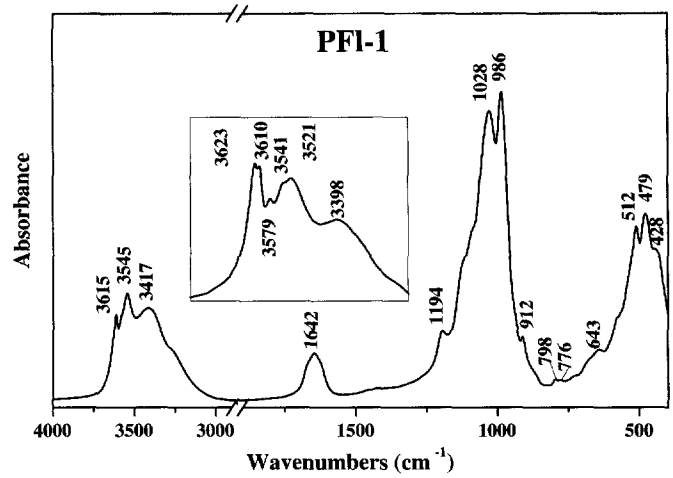

Figure 25. IR spectra of PFl-1 (palygorskite) using 0.5 mg sample/200 mg KBr for 4000–400 cm^{-1}. Insert: 2.0 mg sample/ 200 mg KBr, disk heated overnight at 150°C.

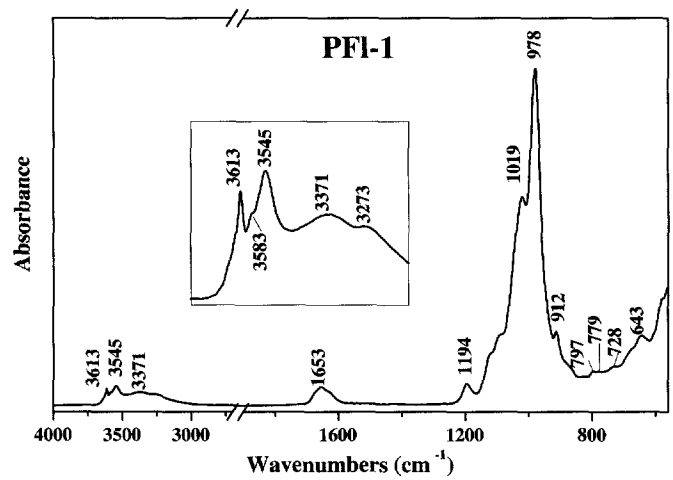

Figure 26. IR spectrum of PFl-1 palygorskite using the ATR technique. Insert: the OH-stretching region.

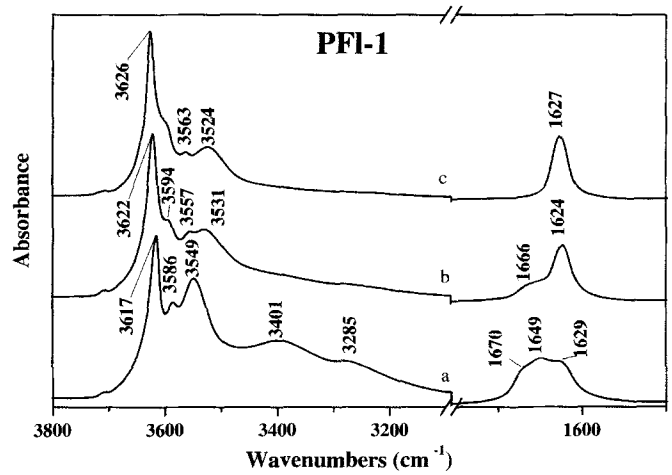

Figure 27. IR spectra of self-supporting film of PFl-1 palygorskite: (a) unheated, (b) heated at 180°C for 0.5 h; and (c) heated at 180°C for 1 h.

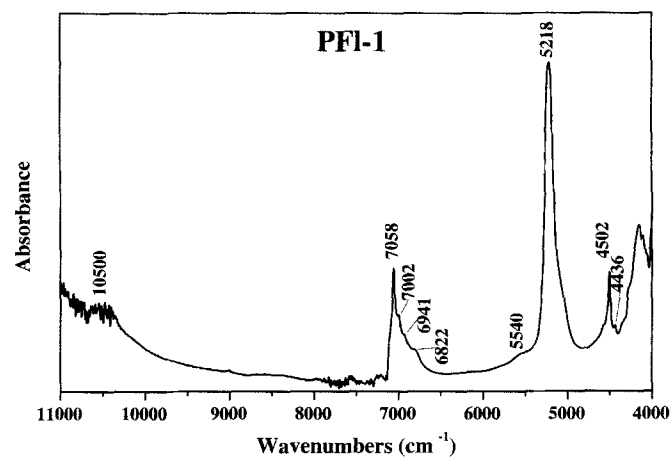

Figure 28. Diffuse-reflectance NIR spectrum of PFl-1 palygorskite.